Electronic Supplementary Material (ESI) for Inorganic Chemistry Frontiers.

Molecular Rotation induced giant, anisotropic negative thermal expansion in a hydrogen-bonded coordination framework

Peng Meng[1]*, *Aidan Brock*[1], *Xiaodong Wang*[2], *Yuting Wang*[1], *John McMurtrie*[1], *Jingsan Xu*[1]*

[1] School of Chemistry and Physics & Centre for Materials Science, Queensland University of Technology, Brisbane, QLD 4000, Australia

[2] Central Analytical Research Facility, Institute for Future Environments, Queensland University of Technology, Brisbane, QLD 4000, Australia

1. Materials synthesis, characterization and measurement

1.1. Materials. Melamine (≥ 99%, Sigma-Aldrich), Cyanuric acid ((≥ 98%, Sigma-Aldrich), Zinc nitrate (≥ 99.5%, Sigma-Aldrich), and ammonia solution (30% in water, Chem-Supply) were used as received without further purification. Ultrapure water was used in all experiments (18.2 MΩ·cm, Synergy UV Water Purification System, Merck Millipore). The solutions of melamine (40 mmol/L) and cyanuric acid (40 mmol/L) were prepared under 60 °C. The solutions of Zinc nitrate (100 mmol/L) and aqueous ammonia (10 wt%) were prepared under ambient environment in the laboratory.

1.2. Preparation of CA-M-Zn crystals. 4.5 mL cyanuric acid solution (40 mM) were mixed with 2 mL $Zn(NO_3)_2$ solution (100 mM) in a 15 mL glass vial, followed by the addition of 3 mL melamine solution (40 mM). The vial was capped and put in a dark closet at room temperature. Transparent crystals started to form within 1 day. The addition of melamine could be in solution or solids, and the initial molar ratio of CA to M could also be random. The outcome of the crystallization is exclusive.

1.3. Powder X-ray diffraction. The crystals were first washed by de-ionized water, then rinsed by ethanol at room temperature for quick drying and grinded into powders. The powder X-ray diffraction (PXRD) patterns were obtained on a Rigaku Smartlab with oxford heating-cooling accessory using Cu Kα radiation (λ = 1.5406 Å) working at 40 mA and 40 kV with a resolution of 0.01° (2θ). Cyclic heating/cooling PXRD for lattice refinement were also

performed in the same instrument by sealing crystallites into a quartz capillary, with equilibrium time of 15 minutes at each temperature.

1.4. PXRD pattern refinement method. The calculation of PXRD patterns from crystal structures and the comparison with the PXRD patterns were conducted in DIFFRAC.TOPAS v6. Cell parameters from in-situ PXRD patterns were obtained by sequential refinements in DIFFRAC.TOPAS v6 with a Macro written by the third author.

1.5. Single crystal X-ray structure determination. A single crystal of CAM-Zn was coated in Paratone N oil and mounted on a nylon loop for collection. SCXRD data for structural determination were collected on Xcalibur, Sapphire3, Gemini ultra (λ = 1.54184 Å). And in situ SCXRD data were collected on XtaLAB Synergy, Dualflex, Pilatus 300K (λ = 0.71073 Å). All data were processed in CrysAlis Pro[1].Structure solutions were obtained using SHELXT[2] and refined using SHELXL[3] implemented within the Olex2 graphical interfacel[4]. All full-occupancy non-hydrogen models were refined anisotropically, while hydrogen atoms were placed in idealised positions and refined using a riding model on appropriate atoms.

Table S1. Crystal data and structure refinement for CA-M-Zn.

Identification code	CA-M-Zn
Empirical formula	$C_{15}H_{42.34}N_{25}O_{15.66}Zn_2$
Formula weight	954.45
Temperature/K	173.00(14)
Crystal system	monoclinic
Space group	P2/c
a/Å	9.5713(2)
b/Å	6.93400(10)
c/Å	29.0393(5)
α/°	90
β/°	93.711(2)
γ/°	90
Volume/Å^3	1923.22(6)
Z	2
ρ_{calc}g/cm^3	1.648
μ/mm^{-1}	2.396
F(000)	985.0
Crystal size/mm^3	0.2 × 0.2 × 0.1
Radiation	Cu Kα (λ = 1.54184)
2Θ range for data collection/°	10.76 to 128.346
Index ranges	-11 ≤ h ≤ 11, -7 ≤ k ≤ 8, -32 ≤ l ≤ 33
Reflections collected	18723
Independent reflections	3177 R_{int} = 0.0275, R_{sigma} = 0.0175
Data/restraints/parameters	3177/2/307
Goodness-of-fit on F^2	1.122
Final R indexes I>=2σ (I)	R_1 = 0.0337, wR_2 = 0.1012
Final R indexes all data	R_1 = 0.0347, wR_2 = 0.1022
Largest diff. peak/hole / e Å^{-3}	1.15/-0.30

Table S2. Variable temperature SCXRD study raw data.

Temperature/K	150.00(10)	200.02(10)	250.01(10)	280.01(10)	290.00(10)
Crystal system	monoclinic	monoclinic	monoclinic	monoclinic	monoclinic
Space group	P2/c	P2/c	P2/c	P2/c	P2/c
a/Å	9.5910(3)	9.6009(3)	9.6144(3)	9.6115(4)	9.6061(4)
b/Å	6.9388(2)	6.9496(2)	6.9595(2)	6.9612(3)	6.9546(3)
c/Å	29.0162(8)	29.0452(8)	29.0893(8)	29.1217(9)	29.1266(9)
α/°	90	90	90	90	90
β/°	93.547(2)	93.638(2)	93.720(3)	93.780(3)	93.692(3)
γ/°	90	90	90	90	90
Volume/Å^3	1927.33(10)	1934.06(10)	1942.31(10)	1944.22(13)	1941.81(13)
ρ_{calc}g/cm^3	1.673	1.667	1.660	1.658	1.660
μ/mm^{-1}	1.933	1.927	1.918	1.917	1.919
F(000)	990.0	990.0	990.0	990.0	990.0
2Θ range for data collection/°	4.954 to 66.918	4.946 to 66.678	4.936 to 66.786	4.932 to 66.758	4.938 to 66.832
Reflections collected	28730	29054	29162	29135	29214
Independent reflections	6386 R_{int} = 0.0846, R_{sigma} = 0.0598	6412 R_{int} = 0.0825, R_{sigma} = 0.0578	6451 R_{int} = 0.0815, R_{sigma} = 0.0579	6443 R_{int} = 0.0818, R_{sigma} = 0.0604	6443 R_{int} = 0.0905, R_{sigma} = 0.0639
Data/restraints/parameters	6386/0/234	6412/0/234	6451/0/234	6443/0/234	6443/0/234
Goodness-of-fit on F^2	0.860	1.096	1.091	1.115	1.113
Final R indexes I>=2σ (I)	R_1 = 0.0591, wR_2 = 0.2053	R_1 = 0.0564, wR_2 = 0.1448	R_1 = 0.0551, wR_2 = 0.1472	R_1 = 0.0584, wR_2 = 0.1597	R_1 = 0.0642, wR_2 = 0.1808
Final R indexes all data	R_1 = 0.0731, wR_2 = 0.2194	R_1 = 0.0708, wR_2 = 0.1508	R_1 = 0.0719, wR_2 = 0.1528	R_1 = 0.0784, wR_2 = 0.1661	R_1 = 0.0862, wR_2 = 0.1897
Largest diff. peak/hole / e Å^{-3}	1.43/-0.54	1.55/-0.53	1.43/-0.54	1.29/-0.51	1.48/-0.53

Temperature/K	300.00(10)	310.00(10)	320.00(10)	325.00(10)	330.00(10)
Crystal system	monoclinic	monoclinic	monoclinic	monoclinic	monoclinic
Space group	P2/c	P2/c	P2/c	P2/c	P2/c
a/Å	9.6002(4)	9.5988(4)	9.6010(5)	9.6114(7)	9.6134(7)
b/Å	6.9504(3)	6.9453(3)	6.9455(4)	6.9454(4)	6.9448(4)
c/Å	29.1051(10)	29.0622(11)	28.9943(14)	28.8982(18)	28.8189(17)
α/°	90	90	90	90	90
β/°	93.474(3)	93.108(3)	92.476(4)	91.564(5)	90.731(5)
γ/°	90	90	90	90	90
Volume/Å^3	1938.48(13)	1934.63(14)	1931.64(18)	1928.4(2)	1923.9(2)
ρ_{calc}g/cm^3	1.663	1.667	1.669	1.672	1.676
μ/mm^{-1}	1.922	1.926	1.929	1.932	1.937
F(000)	990.0	990.0	990.0	990.0	990.0
2Θ range for data collection/°	4.948 to 66.946	4.964 to 66.73	4.992 to 66.986	5.028 to 66.722	5.064 to 66.974
Reflections collected	29140	29045	28736	28318	28459
Independent reflections	6421 R_{int} = 0.1002, R_{sigma} = 0.0684	6394 R_{int} = 0.0985, R_{sigma} = 0.0722	6402 R_{int} = 0.1107, R_{sigma} = 0.0815	6379 R_{int} = 0.1191, R_{sigma} = 0.0910	6358 R_{int} = 0.1227, R_{sigma} = 0.0900
Data/restraints/parameters	6421/0/234	6394/0/234	6402/0/234	6379/0/234	6358/0/234
Goodness-of-fit on F^2	1.122	1.069	1.074	1.066	1.038
Final R indexes I>=2σ (I)	R_1 = 0.0684, wR_2 = 0.1951	R_1 = 0.0676, wR_2 = 0.1863	R_1 = 0.0759, wR_2 = 0.2053	R_1 = 0.0858, wR_2 = 0.2233	R_1 = 0.0922, wR_2 = 0.2653
Final R indexes all data	R_1 = 0.0917, wR_2 = 0.2044	R_1 = 0.0946, wR_2 = 0.1970	R_1 = 0.1064, wR_2 = 0.2165	R_1 = 0.1224, wR_2 = 0.2374	R_1 = 0.1287, wR_2 = 0.2847
Largest diff. peak/hole / e Å^{-3}	1.23/-0.55	0.95/-0.72	1.14/-0.68	0.84/-0.74	1.09/-1.29

Temperature/K	335.00(10)	340.00(10)	345.00(10)	350.00(10)	355.00(10)
Crystal system	monoclinic	monoclinic	monoclinic	monoclinic	monoclinic
Space group	P2/c	P2/c	P2/c	P2/c	P2/c
a/Å	9.6173(5)	9.6204(5)	9.6162(5)	9.6232(5)	9.6271(6)
b/Å	6.9458(3)	6.9456(3)	6.9418(3)	6.9478(3)	6.9548(4)
c/Å	28.7789(12)	28.7738(10)	28.7773(10)	28.8132(10)	28.8430(12)
α/°	90	90	90	90	90
β/°	90.232(4)	90.034(4)	90.116(3)	90.030(4)	90.156(4)
γ/°	90	90	90	90	90
Volume/Å^3	1922.41(15)	1922.65(15)	1920.99(15)	1926.45(15)	1931.16(18)
ρ_{calc}g/cm^3	1.677	1.677	1.678	1.674	1.670
μ/mm^{-1}	1.938	1.938	1.940	1.934	1.930
F(000)	990.0	990.0	990.0	990.0	990.0
2Θ range for data collection/°	5.086 to 66.866	5.092 to 66.88	5.09 to 66.936	5.09 to 66.91	5.082 to 66.948
Reflections collected	28690	28859	29022	28982	28906
Independent reflections	6374 R_{int} = 0.1239, R_{sigma} = 0.0910	6375 R_{int} = 0.1194, R_{sigma} = 0.0875	6389 R_{int} = 0.1199, R_{sigma} = 0.0880	6395 R_{int} = 0.1281, R_{sigma} = 0.0935	6403 R_{int} = 0.1263, R_{sigma} = 0.0954
Data/restraints/parameters	6374/0/234	6375/0/234	6389/0/235	6395/0/234	6403/0/234
Goodness-of-fit on F^2	1.070	1.050	1.028	1.037	1.004
Final R indexes I>=2σ (I)	R_1 = 0.0957, wR_2 = 0.2723	R_1 = 0.0914, wR_2 = 0.2571	R_1 = 0.0908, wR_2 = 0.2522	R_1 = 0.0961, wR_2 = 0.2693	R_1 = 0.0967, wR_2 = 0.2732
Final R indexes all data	R_1 = 0.1324, wR_2 = 0.2906	R_1 = 0.1285, wR_2 = 0.2755	R_1 = 0.1274, wR_2 = 0.2718	R_1 = 0.1353, wR_2 = 0.2906	R_1 = 0.1408, wR_2 = 0.2981
Largest diff. peak/hole / e Å^{-3}	1.25/-1.47	1.24/-1.45	0.93/-1.44	1.03/-1.63	1.10/-1.65

Temperature/K	360.00(10)	365.00(10)	370.00(10)	375.00(10)
Crystal system	monoclinic	monoclinic	monoclinic	monoclinic
Space group	P2/c	P2/c	P2/c	P2/c
a/Å	9.6255(6)	9.6250(6)	9.6281(7)	9.6290(7)
b/Å	6.9592(4)	6.9587(4)	6.9664(4)	6.9689(4)
c/Å	28.8493(12)	28.8587(12)	28.8775(14)	28.8838(14)
α/°	90	90	90	90
β/°	90.396(4)	90.597(4)	90.664(5)	90.775(5)
γ/°	90	90	90	90
Volume/Å^3	1932.45(18)	1932.78(18)	1936.8(2)	1938.0(2)
ρ_{calc}g/cm^3	1.668	1.668	1.665	1.664
μ/mm^{-1}	1.928	1.928	1.924	1.923
F(000)	990.0	990.0	990.0	990.0
2Θ range for data collection/°	5.072 to 66.792	5.064 to 66.832	5.058 to 66.794	5.054 to 66.798
Reflections collected	28971	29104	29112	29184
Independent reflections	6399 R_{int} = 0.1245, R_{sigma} = 0.0959	6405 R_{int} = 0.1272, R_{sigma} = 0.0958	6417 R_{int} = 0.1285, R_{sigma} = 0.0969	6429 R_{int} = 0.1291, R_{sigma} = 0.0994
Data/restraints/parameters	6399/0/235	6405/0/234	6417/0/234	6429/0/234
Goodness-of-fit on F^2	1.004	0.998	1.003	1.011
Final R indexes I>=2σ (I)	R_1 = 0.0960, wR_2 = 0.2717	R_1 = 0.0970, wR_2 = 0.2775	R_1 = 0.0972, wR_2 = 0.2824	R_1 = 0.0977, wR_2 = 0.2792
Final R indexes all data	R_1 = 0.1404, wR_2 = 0.2953	R_1 = 0.1428, wR_2 = 0.3032	R_1 = 0.1458, wR_2 = 0.3086	R_1 = 0.1487, wR_2 = 0.3069
Largest diff. peak/hole / e Å^{-3}	1.02/-1.44	1.25/-1.28	1.22/-1.16	1.28/-1.13

Table S3. Numeric data in Figure 2b.

Compound	α_v (10^{-6} K^{-1})	ΔT	Ref.
Oxides			
ZrW_2O_8	-21.9	1049.7	5
α-HfW_2O_8	-26.4	378	6
β-HfW_2O_8	-16.5	92	6
γ-$ZrMo_2O_8$	-15.0	562	7
γ-$HfMo_2O_8$	-12.0	496	8
α-$Zr_{0.7}Sn_{0.3}W_2O_8$	-40.6	100	9
β-$Zr_{0.7}Sn_{0.3}W_2O_8$	-18.7	450	9
α-$Zr_{0.95}Ti_{0.05}W_2O_8$	-30.0	105	10
β-$Zr_{0.95}Ti_{0\cdot05}W_2O_8$	-13.5	168	10
$Zr_{0.96}M_{0.04}W_2O_{8-0.02}$(M = Eu^{3+}, Er^{3+} and Yb^{3+})	-30.9	70	11
$ZrW_{1.8}V_{0.2}O_{7.9}$	-29.1	74	12
$ZrW_{1.8}V_{0.2}O_{7.9}$	-4.8	175	12
ZrV_2O_7	-20.1	498	13
ZrV_2O_7	-75.5	168	13
ThP_2O_7	-10.5	501	14
CeP_2O_7	-5.7	360	15
$Zr_{0.70}V_{1.33}Mo_{0.67}O_{6.73}$	-11.3	510	16
$Sc_2W_3O_{12}$	-6.7	1190	17
$Dy_2W_3O_{12}$	-26.0	350	18
$Y_2W_3O_{12}$	-21.0	1358	19
$Er_2W_3O_{12}$	-20.2	600	20
$Yb_2W_3O_{12}$	-19.1	600	20
$Lu_2W_3O_{12}$	-18.5	600	20
$Y_2Mo_3O_{12}$	-37.8	770	21
$Er_2Mo_3O_{12}$	-22.7	775	22
$Yb_2Mo_3O_{12}$	-18.1	775	22
$Lu_2Mo_3O_{12}$	-18.1	775	22
$Sc_2Mo_3O_{12}$	-18.9	775	22
$NbPO_5$	-11.0	300	23
$TaPO_5$	-1.7	400	23
$TaVO_5$	-8.9	580	24
$TaVO_5$	-21.9	200	24
$NbVO_5$	-6.6	575	25
$TaAs_{0.1}V_{0.9}O_5$	-17.5	480	23
ReO_3	-1.8	80	24
SiO_2 (β-cristobalite)	*-6.9*	*548*	25
Cu_2O	-7.2	231	26
Ag_2O	-21	145	27
Ag_2O	-27.1	173	26
$AlPO_4$-17	-35.1	282	28
H-ZSM-5	-27	800	29
$Zn_2V_2O_7$	-17.9	300	30
α-$Cu_2V_2O_7$	-10.2	375	31
Fluorides			
$CaZrF_6$	-26.5	1163	32
$MnZrF_6$	-13.4	373	33
$FeZrF_6$	-9.7	373	33

$MgZrF_6$	-2.4	373	34
$CaHfF_6$	-45.3	288	32
$CaNbF_6$	-36.5	775	35
$TiZrF_6$	-6.1	323	36
$YbZrF_7$	-6.0	132	37
Cyanides			
$Zn(CN)_2$	-50.7	350	38
$Cd(CN)_2$ (double-network)	-61.2	225	38
$Cd(CN)_2$ (single-network)	-100	225	39
$Zn[Ag(CN)_2]_2$	-13.6	275	40
$AgB(CN)_4$	-40.0	500	41
$CuB(CN)_4$	-9.2	300	41
$YFe(CN)_6$	-33.7	225	42
$FeCo(CN)_6$	-4.4	295.8	43
$GaFe(CN)_6$	-11.9	375	44
$FeFe(CN)_6$	-12.8	350	45
$ScCo(CN)_6$	-19.8	575	46
$TiCo(CN)_6$	-12.2	375	47
$LaCo(CN)_6$	-43.9	400	48
$SmCo(CN)_6$	-37.4	400	48
$HoCo(CN)_6$	-30.2	400	48
$LuCo(CN)_6$	-27.2	400	48
$YCo(CN)_6$	-31.6	400	48
$ErCo(CN)_6$	-27.0	275	49
$CsCd[Fe(CN)_6]\cdot 0.5H_2O$	-26.4	200	50
$Cs_{0.7}Ni[Fe(CN)_6]_{0.9}\cdot 2.9H_2O$	-1.2	200	50
$Cs_{0.97}Cu[Fe(CN)_6]_{0.99}\cdot 1.1H_2O$	-6.3	200	50
$Cs_{0.91}Ni[Fe(CN)_6]_{0.97}\cdot 0.4H_2$	-12.3	200	50
$Rb_{0.78}Fe[Fe(CN)_6]_{0.83}\cdot 2.8H_2O$	-6.3	200	50
$Rb_{0.64}Zn[Fe(CN)_6]_{0.88}\cdot 2.3H_2O$	-17.7	200	50
$CdPt(CN)_6$	-30.1	140	51
$MnPt(CN)_6$	-19.7	200	51
$FePt(CN)_6$	-12.0	215	51
$CoPt(CN)_6$	-4.8	250	51
$NiPt(CN)_6$	-3.1	230	51
$ZnPt(CN)_6$	-10.6	300	51
$Mn_3Co(CN)_6]_2\cdot 12H_2O$	-87.6	175	52
$Fe_3Co(CN)_6]_2\cdot 12H_2O$	-58.8	175	52
$Co_3Co(CN)_6]_2\cdot 12H_2O$	-119.1	175	52
$Ni_3Co(CN)_6]_2\cdot 12H_2O$	-83.0	175	52
$Cu_3Co(CN)_6]_2\cdot 12H_2O$	-58.7	175	52
$Zn_3Co(CN)_6]_2\cdot 12H_2O$	-89.1	175	52
$Fe_3Fe(CN)_6]_2\cdot 16H_2O$	-29.7	175	52
$Cu_3Fe(CN)_6]_2\cdot 16H_2O$	-59.7	175	52
$Zn_3Fe(CN)_6]_2\cdot 16H_2O$	-118.8	175	52
MOFs			
MOF-5	-39.3	420	53
HKUST-1	-12.3	420	54
UiO-66(Zr)	-97	180	55

MIL-68(In)	-12.3	475	56
$Zn_8(SiO_4)(m\text{-}BDC)_6$	-4.4	375	57
Cu-TDPAT	-19.7	400	58
$M_2C_4O_4{\cdot}2H_2O$ (M = Zn, Cd)	-13.9	250	59

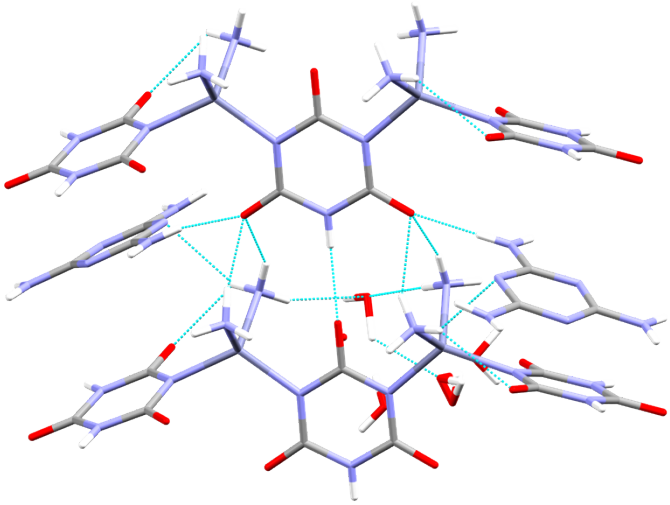

Figure S1. Auxiliary H-bonds between NH_3 and M(CA).

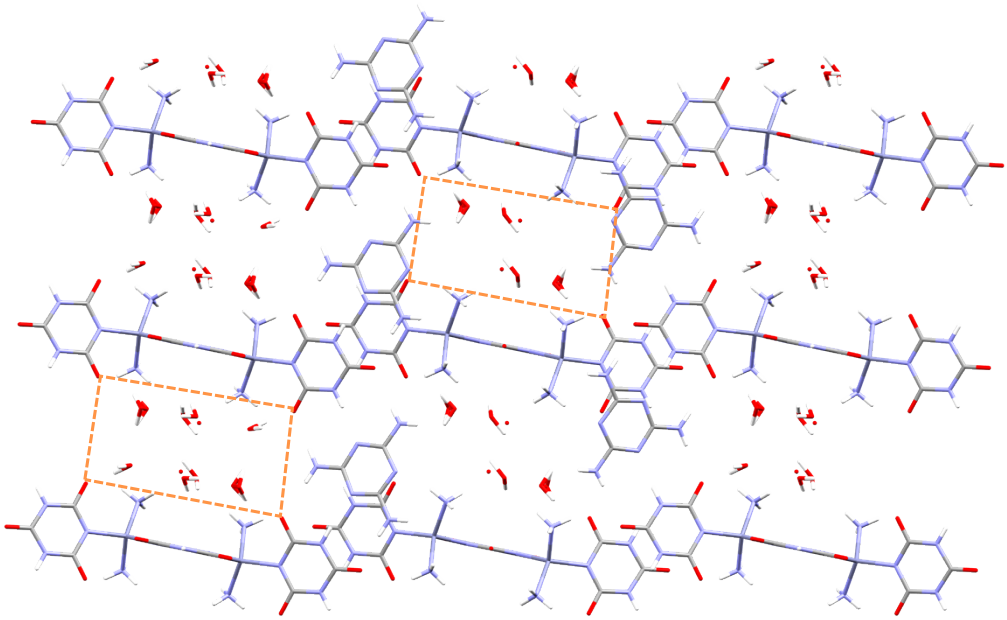

Figure S2. Water molecules filling the 1D channels.

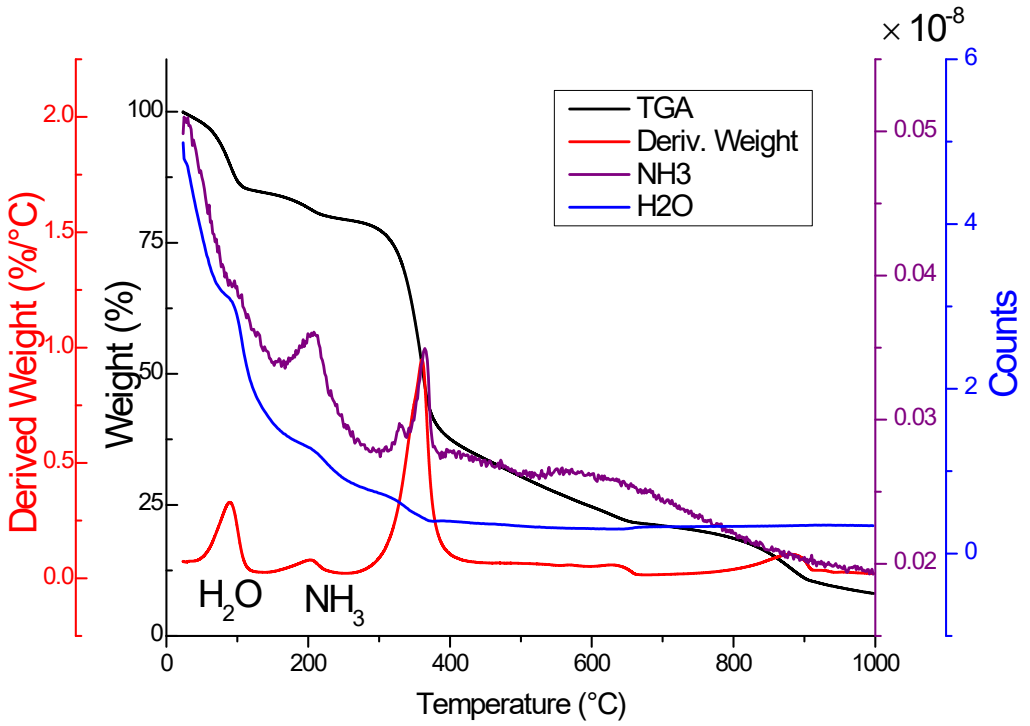

Figure S3. TGA-MS result of CAM-Zn crystal.

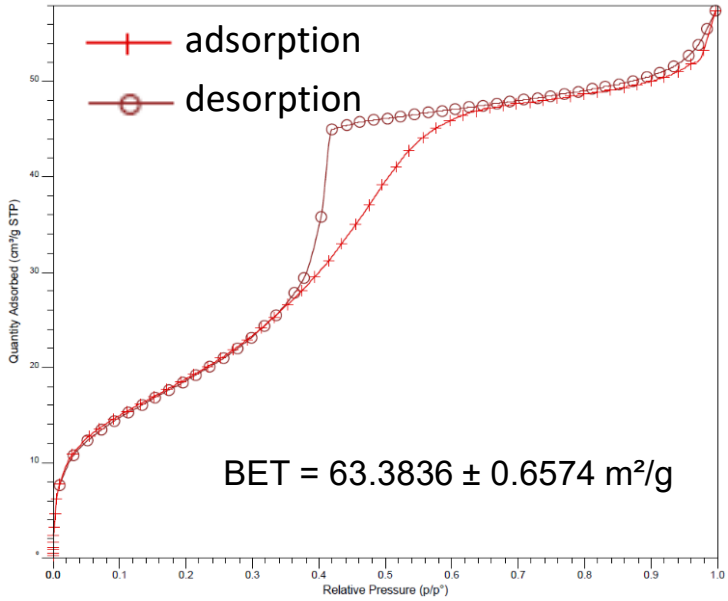

Figure S4. N_2 Adsorption/desorption curves. Degas temperature: 105 ℃.

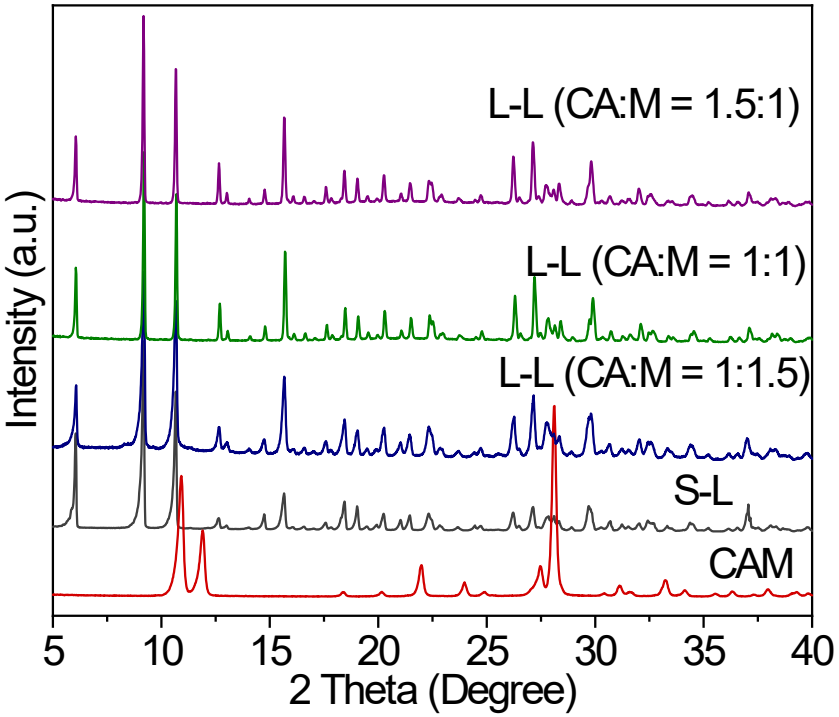

Figure S5. PXRD patterns of crystals obtained at different conditions. L-L means all reactants were in solutions state at the commencement of reaction; following is the molar ratio of CA:M. S-L means that the M added in the reaction system was particles (without dissolved) and CA was in solution state (the amount of M do not affect the outcome).

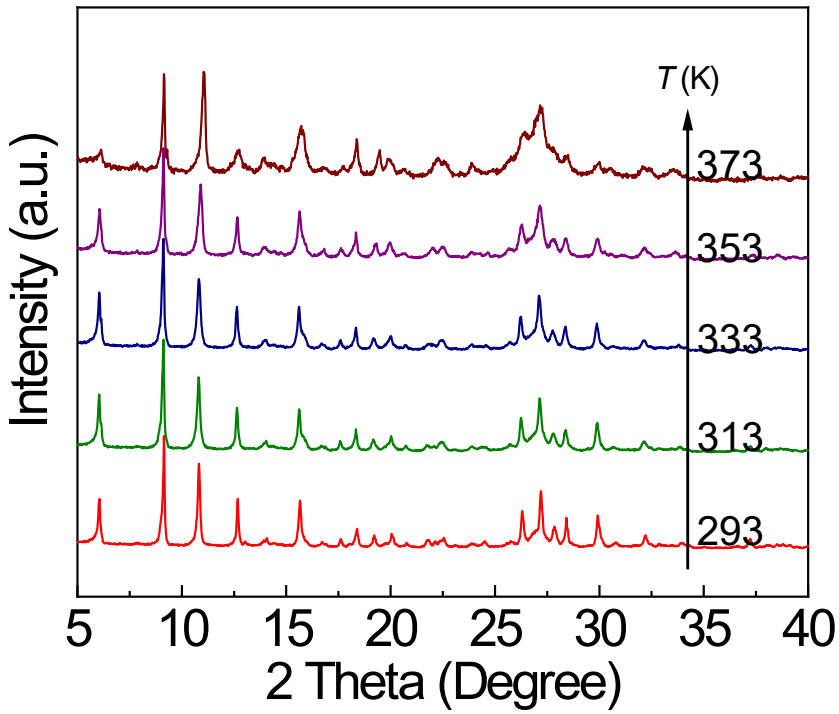

Figure S6. PXRD patterns at varied temperatures.

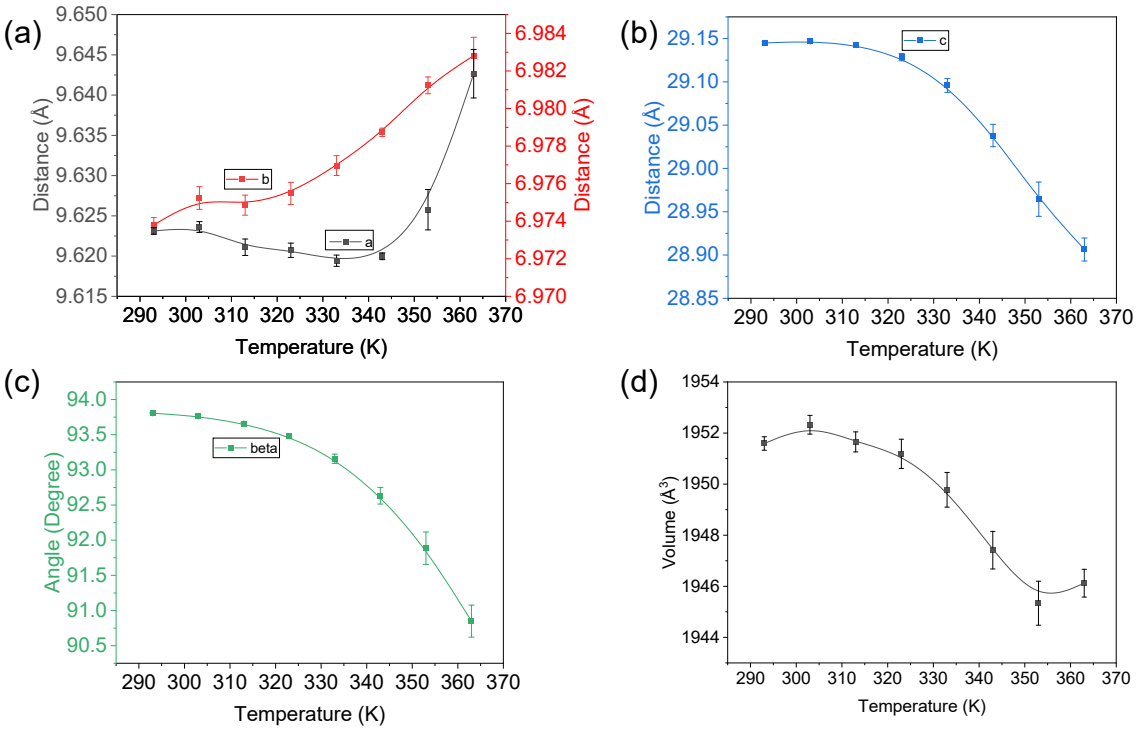

Figure S7. unit cell parameters refined from in-situ PXRD patterns: (a) *a* and *b* axis, (b) *c* axis, (c) beta angle, (d) volume change.

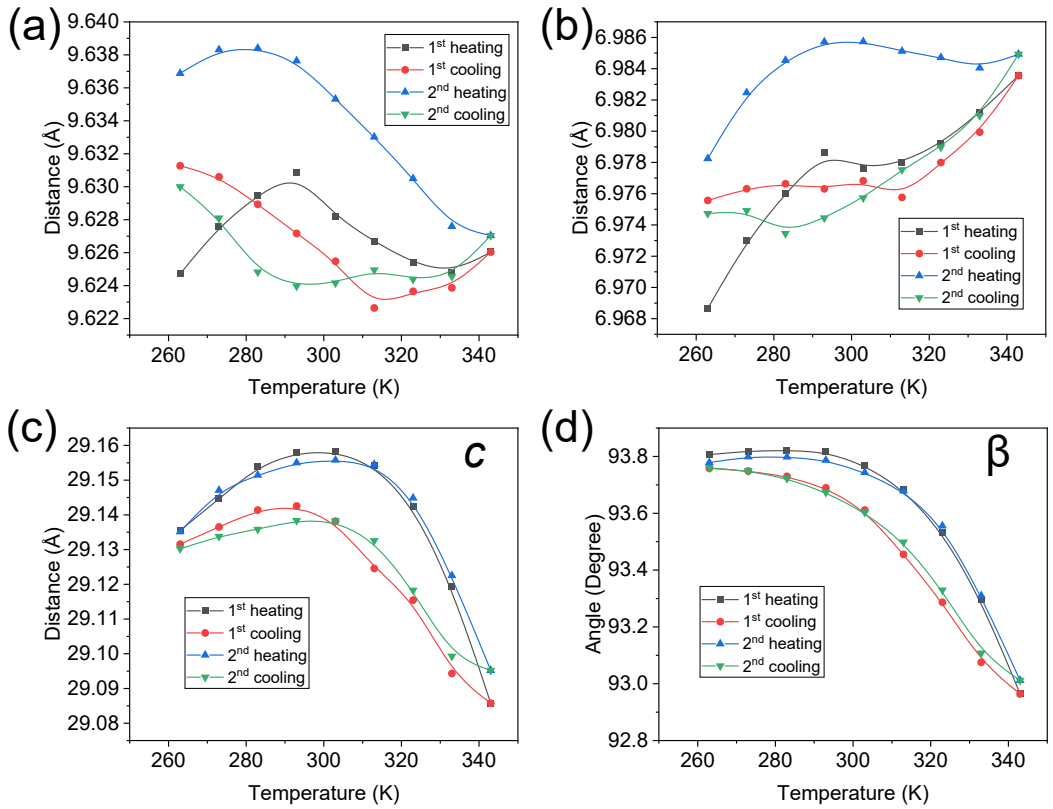

Figure S8. the length change of (a) *a* axis, (b) *b* axis, (c) axis, (d) β angle upon cyclic heating/cooling.

Figure S9. illustration of θ_2 and ω_2 rotations of CA02 with respect to Zn.

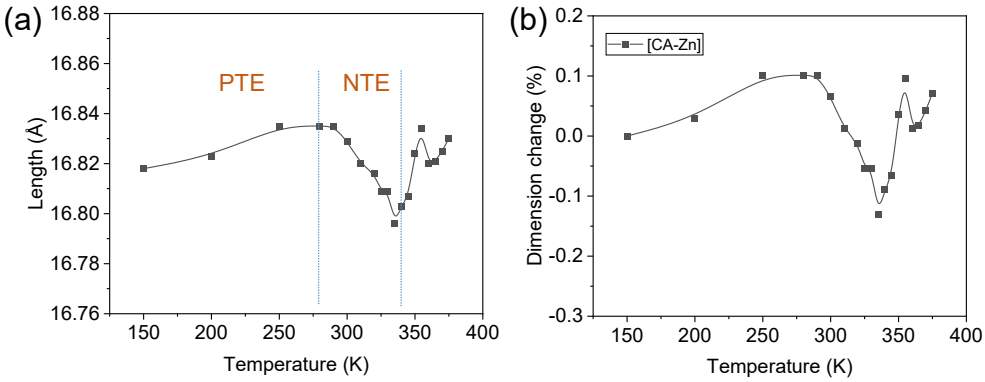

Figure S10. (a) Length change of coordination subunits CA-Zn-CA-Zn-CA with respect to temperature (measured between the two farthest oxygen atoms) and (b) the corresponding dimension change.

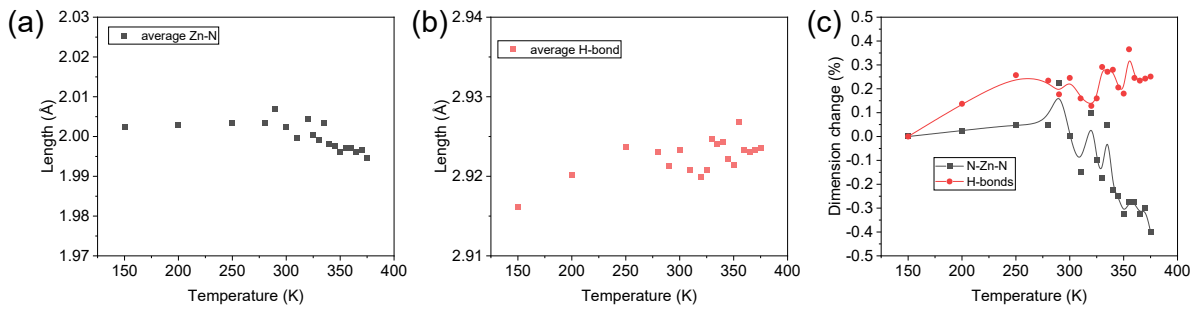

Figure S11. (a) Average length of Zn-N(CA) bonds, (b) average length of triple H-bonds between M-CA01, (c) the corresponding dimension change.

Reference

1. Diffraction, R. O. CrysAlis Pro, 40_64.53a; Rigaku Oxford Diffraction: 2019.
2. Sheldrick, G. M., SHELXT - Integrated space-group and crystal-structure determination. Acta Crystallographica a-Foundation and Advances 2015, 71, 3-8.
3. Sheldrick, G. M., A short history of SHELX. Acta Crystallographica Section A 2008, 64, 112-122.
4. Dolomanov, O. V.; Bourhis, L. J.; Gildea, R. J.; Howard, J. A. K.; Puschmann, H., OLEX2: a complete structure solution, refinement and analysis program. Journal of Applied Crystallography 2009, 42, 339-341.
5. T. Mary, J. Evans, T. Vogt, A. Sleight, Science 272 (1996) 90–92.
6. Y. Yamamura, N. Nakajima, T. Tsuji, Phys. Rev. B 64 (2001) 184109.
7. C. Lind, A.P. Wilkinson, Z. Hu, S. Short, J.D. Jorgensen, Chem. Mater. 10 (1998) 2335–2337.
8. C. Lind, Negative thermal expansion materials related to cubic zirconium tungstate, Georgia Institute of Technology, 2001.
9. C. De Meyer, F. Bouree, J.S. Evans, K. De Buysser, E. Bruneel, I. Van Driessche, S. Hoste, J. Mater. Chem. 14 (2004) 2988–2994.
10. K. De Buysser, I. Van Driessche, B.V. Putte, J. Schaubroeck, S. Hoste, J. Solid State Chem. 180 (2007) 2310–2315.
11. H.H. Li, J.S. Han, H. Ma, L. Huang, X.H. Zhao, J. Solid State Chem. 180 (2007) 852–857.
12. X. Chen, F. Guo, X. Deng, J. Tao, H. Ma, X. Zhao, J. Alloys Compd. 537 (2012) 227–231.
13. R. Withers, J. Evans, J. Hanson, A. Sleight, J. Solid State Chem. France 137 (1998) 161–167.
14. G. Wallez, P.E. Raison, N. Dacheux, N. Clavier, D. Bykov, L. Delevoye, K. Popa, D. Bregiroux, A.N. Fitch, R.J. Konings, Inorg. Chem. 51 (2012) 4314–4322.
15. K. White, P.L. Lee, P.J. Chupas, K. Chapman, E.A. Payzant, A.C. Jupe, W. Bassett, C.S. Zha, A.P. Wilkinson, Chem. Mater. 20 (2008) 3728–3734.
16. M. Zhang, Y. Mao, J. Guo, W. Zhou, M. Chao, N. Zhang, M. Yang, X. Kong, X. Kong, E. Liang, RSC Adv. 7 (2017) 3934–3940.
17. T. Mary, A. Sleight, J. Mater. Res. 14 (1999) 912–915.
18. W. Cao, Q. Li, K. Lin, Z. Liu, J. Deng, J. Chen, X. Xing, RSC Adv. 6 (2016) 96275– 96280.
19. P. Forster, A. Sleight, Int. J. Inorg. Mater. 1 (1999) 123–127.
20. S. Sumithra, A. Tyagi, A. Umarji, Mater. Sci. Eng., B 116 (2005) 14–18.
21. B. Marinkovic, P. Jardim, R. De Avillez, F. Rizzo, Solid State Sci. 7 (2005) 1377– 1383.
22. S. Sumithra, A. Umarji, Solid State Sci. 8 (2006) 1453–1458.
23. T.G. Amos, Negative thermal expansion in $AOMO_4$ compounds, Oregon State University, 2000.
24. X. Wang, Q. Huang, J. Deng, R. Yu, J. Chen, X. Xing, Inorg. Chem. 50 (2011) 2685–2690.
25. J. Wang, J. Deng, R. Yu, J. Chen, X. Xing, Dalton Trans. 40 (2011) 3394–3397.
26. W. Tiano, M. Dapiaggi, G. Artioli, J. Appl. Crystallogr. 36 (2003) 1461–1463.
27. B.J. Kennedy, Y. Kubota, K. Kato, Solid State Commun. 136 (2005) 177–180.
28. M.P. Attfield, A.W. Sleight, Chem. Mater. 10 (1998) 2013–2019.
29. B. Marinkovic, P. Jardim, A. Saavedra, L. Lau, C. Baehtz, R. De Avillez, F. Rizzo, Micropor. Mesopor. Mat. 71 (2004) 117–124.

30. M. Rotermel, T. Krasnenko, Crystallogra. Rep. 62 (2017) 703–709.
31. N. Shi, A. Sanson, A. Venier, L. Fan, C. Sun, X. Xing, J. Chen, Chem. Comm. 56 (2020) 10666–10669.
32. J.C. Hancock, K.W. Chapman, G.J. Halder, C.R. Morelock, B.S. Kaplan, L.C. Gallington, A. Bongiorno, C. Han, S. Zhou, A.P. Wilkinson, Chem. Mater. 27 (2015) 3912–3918.
33. L. Hu, J. Chen, J. Xu, N. Wang, F. Han, Y. Ren, Z. Pan, Y. Rong, R. Huang, J. Deng, J. Am. Chem. Soc. 138 (2016) 14530–14533.
34. J. Xu, L. Hu, Y. Song, F. Han, Y. Qiao, J. Deng, J. Chen, X. Xing, J. Am. Ceram. Soc. 100 (2017) 5385–5388.
35. B.R. Hester, J.C. Hancock, S.H. Lapidus, A.P. Wilkinson, Chem. Mater. 29 (2017) 823–831.
36. C. Yang, Y. Zhang, J. Bai, B. Qu, P. Tong, M. Wang, J. Lin, R. Zhang, H. Tong, Y. Wu, J. Mater. Chem. C 6 (2018) 5148–5152.
37. J.O. Ticknor, B.R. Hester, J.W. Adkins, W. Xu, A.A. Yakovenko, A.P. Wilkinson, Chem. Mater. 30 (2018) 3071–3077.
38. A.L. Goodwin, C.J. Kepert, Phys. Rev. B 71 (2005) 140301.
39. A.E. Phillips, A.L. Goodwin, G.J. Halder, P.D. Southon, C.J. Kepert, Angew. Chem. Int. Ed. 47 (2008) 1396–1399.
40. A.L. Goodwin, B.J. Kennedy, C.J. Kepert, J. Am. Chem. Soc. 131 (2009) 6334– 6335.
41. Q. Gao, J. Wang, A. Sanson, Q. Sun, E. Liang, X. Xing, J. Chen, J. Am. Chem. Soc. 142 (2020) 6935–6939.
42. Q. Gao, J. Chen, Q. Sun, D. Chang, Q. Huang, H. Wu, A. Sanson, R. Milazzo, H. Zhu, Q. Li, Angew. Chem. Int. Ed. 56 (2017) 9023–9028.
43. S. Margadonna, K. Prassides, A.N. Fitch, J. Am. Chem. Soc. 126 (2004) 15390– 15391.
44. Q. Gao, N. Shi, Q. Sun, A. Sanson, R. Milazzo, A. Carnera, H. Zhu, S.H. Lapidus, Y. Ren, Q. Huang, Inorg. Chem. 57 (2018) 10918–10924.
45. N. Shi, Q. Gao, A. Sanson, Q. Li, L. Fan, Y. Ren, L. Olivi, J. Chen, X. Xing, Dalton Trans. 48 (2019) 3658–3663.
46. Q. Gao, Y. Sun, N. Shi, R. Milazzo, S. Pollastri, L. Olivi, Q. Huang, H. Liu, A. Sanson, Q. Sun, Scr. Mater. 187 (2020) 119–124.
47. Y. Li, Q. Gao, D. Chang, P. Sun, J. Liu, Y. Jia, E. Liang, Q. Sun, J. Phys, Condens. Mat. 32 (2020) 455703.
48. S.G. Duyker, V.K. Peterson, G.J. Kearley, A.J. Ramirez-Cuesta, C.J. Kepert, Angew. Chem. Int. Ed. 52 (2013) 5266–5270.
49. T. Pretsch, K.W. Chapman, G.J. Halder, C.J. Kepert, Chem. Comm. (2006) 1857– 1859.
50. T. Matsuda, J. Kim, K. Ohoyama, Y. Moritomo, Phys. Rev. B 79 (2009) 172302.
51. K.W. Chapman, P.J. Chupas, C.J. Kepert, J. Am. Chem. Soc. 128 (2006) 7009– 7014.
52. S. Adak, L.L. Daemen, M. Hartl, D. Williams, J. Summerhill, H. Nakotte, J. Solid State Chem. 184 (2011) 2854–2861.
53. N. Lock, Y. Wu, M. Christensen, L.J. Cameron, V.K. Peterson, A.J. Bridgeman, C.J. Kepert, B.B. Iversen, J. Phys. Chem. C 114 (2010) 16181–16186.

54. Y. Wu, A. Kobayashi, G.J. Halder, V.K. Peterson, K.W. Chapman, N. Lock, P.D. Southon, C.J. Kepert, Angew. Chem. Int. Ed. 47 (2008) 8929–8932.
55. M.J. Cliffe, J.A. Hill, C.A. Murray, F.X. Coudert, A.L. Goodwin, Phys. Chem. Chem. Phys. 17 (2015) 11586–11592.
56. Z. Liu, Q. Li, H. Zhu, K. Lin, J. Deng, J. Chen, X. Xing, Chem. Comm. 54 (2018) 5712–5715.
57. Z. Liu, X. Jiang, C. Wang, C. Liu, Z. Lin, J. Deng, J. Chen, X. Xing, Inorg. Chem. Front. 6 (2019) 1675–1679.
58. M. Asgari, I. Kochetygov, H. Abedini, W.L. Queen, Nano Res. (2020) 1–7.
59. Z. Liu, R. Ma, J. Deng, J. Chen, X. Xing, Chem. Mater. 32 (2020) 2893–2898.